CALCULATIONS OF TRANSONIC STEADY STATE AEROELASTIC EFFECTS FOR A CANARD AIRPLANE

N. Agrell and S.G. Hedman
FFA, The Aerodynamic Research Institute of Sweden,
Box 11021, S-161 11 Bromma 11

Abstract

An airplane with supersonic flight capability can be expected to have considerable steady state aeroelastic effects as it operates at high dynamic pressures in a speed range giving large variations of the load distribution.

For calculation of the aerodynamic loading the transonic small perturbation potential method is used. One version has been developed to allow for two wing surfaces with wakes. The method is of sufficient accuracy for aeroelastic studies. The wing deformations are assumed to be linear functions of the load distributions.

The iterative procedure used to solve the transonic small perturbation potential equation in finite difference form is capable of treating the flow field around given wing shapes. As the shape of the elastic wing is, a priori, not known temporary wing shapes have to be determined. These depend on temporary load distributions and are quantified through the deformation matrix of the wing. When external aerodynamic loads are in equilibrium with internal elastic forces the final shape of the wing has been produced.

The results obtained are compared with results from earlier computations and tests.

Symbols

A	matrix of aerodynamic influence coefficients for subsonic flow
b_2	half span of the airplane
c	local chord
C_L	lift coefficient
C_ℓ	rolling moment due to δ_a
C_m	moment coefficient
c_n	sectional normal force coefficient
C_p	pressure coefficient
D	deformation matrix
ℓ	aerodynamic load
M_∞	free stream Mach number
q	dynamic pressure
U_∞	free stream velocity
x,y,z	Cartesian coordinate system
α	angle of attack
α_e	local mean line slope of loaded elastic wing
α_r	local mean line slope of unloaded wing
$\Delta\alpha$	deformation of elastic wing
γ	specific heat ratio
δ	elevon angle
δ_a	aileron angle
ε	scaling factor
η	ratio of aerodynamic coefficients for deformed and undeformed wings
Λ_c	canard sweep angle
Λ_w	main wing sweep angle
Φ	total velocity potential
ϕ	perturbation velocity potential

I. Introduction

The transonic small perturbation potential method available at FFA has been developed to treat two wing surfaces with wakes. The evaluation of steady state aeroelastic effects has been implemented as an option. The vortex roll up and leading edge separation have been neglected.

As a test aeroelastic characteristics have been computed for the SAAB 37 Viggen They have been compared with results from wind tunnel and flight tests but also with earlier computations as reported in the ICAS-paper[1] concerning the same aircraft. It was found that these characteristics varied rapidly in the transonic speed range where no reliable computational methods were available at that time.

Rigid canard-wing interactions at transonic speed have recently been treated by other authors [2].

II Equations and Interior Boundary Conditions

The transonic small disturbance equation is written in ϕ, the disturbance potential

$$\{(1-M_\infty^2)-[3-(2-\gamma)M_\infty^2]M_\infty^2\ \varepsilon\phi_x\}\phi_{xx}+ \\ +\phi_{yy}+\phi_{zz}=0 \qquad (1)$$

where ϕ is defined in terms of the full velocity potential Φ,

$$\Phi(x,y,z) = U_\infty[x + \varepsilon\phi(x,y,z)]$$

with $\varepsilon = \delta^{2/3}/M_\infty$. The equation is transformed into finite difference form and solved by the successive line over relaxation procedure introduced by Murman and Cole[3].

At the wing and canard surfaces no mass flux through the surface, $z(x,y)$, is permitted. This boundary condition is applied at their mean chord planes. It is given[4] by

$$\phi_z = \{\frac{1}{\varepsilon} + (1-M_\infty^2)\phi_x - \frac{1}{2}(3-(2-\gamma))M_\infty^2\varepsilon\phi_x^2\}\frac{dz}{dx} + \phi_y\frac{dz}{dy}$$

For field points adjacent to the body the velocity vector is required to be parallel to the configuration surface and the boundary condition is given by

$$\phi_z = (\frac{1}{\varepsilon} + \phi_x)f_x + \phi_y f_y$$

where $z = f(x,y)$ describes the body surface.

A consistent pressure coefficient[4] has been used

$$C_p = \{-2\varepsilon\phi_x - \varepsilon^2[(1-M_\infty^2)\phi_x^2+\phi_y^2+\phi_z^2] + \varepsilon^3[3-(2-\gamma)M_\infty^2]M_\infty^2\phi_x^3/3\}$$

Across the vortex wakes there will be a jump in the perturbation velocity potential ϕ which will be considered in the calculation as a boundary condition at the grid points neighbouring the wakes.

III. Exterior Boundary Conditions

As the computation domain is rather small the disturbance potential cannot be set equal to zero at the exterior surfaces.

a) Subsonic flow

The potential at the exterior surfaces depends on airplane lift and volume for the three streamwise surfaces. The latter influence may be neglected and the former is estimated from far field expressions derived by Klunker[5]. The bound vortex is positioned along a straight line ($x = XA$, $z = 0$), where XA can be taken as the position of the airplane center of gravity and $z = 0$ is situated vertically midway between the wing and the canard. The spanwise distribution of vorticity equals the sum of wing and canard lift distributions.

At the upstream and downstream planes the influence of the ϕ_{xx} term is small and the two-dimensional Laplace equation is used.

b) Supersonic flow

For supersonic flow the conditions at the outer boundary surfaces are different. The upstream plane is free from influence from the computational domain and all perturbation velocities are zero. The potential at the downstream plane has no influence on the calculations in the interior. At the upper (z= maximum) and lower (z= minimum) streamwise surfaces $d\phi/dz$ is put equal to zero while $d\phi/dy$ is put equal to zero at the third streamwise surface (y= maximum).

IV. The Treatment of Steady State Aeroelastic Effects

The wing deformation is expressed as rotations, $\Delta\alpha$, normal to the x,z-plane due to vertical loads, ℓ. The deformations are for small wing deflections linear functions ot the loads

$$\{\Delta\alpha\} = [D]\{\ell\} \qquad (2)$$

where D is the deformation matrix evaluated from measurements on the real wing.

$$\{\alpha_e\} = \{\alpha_r\} + \{\Delta\alpha\} \qquad (3)$$

α_r is the mean line slope of the wing when unloaded, and α_e is the local angle of attack for the same elastic wing when loaded.

The aerodynamic relation between load, ℓ, and α_e is linear in subsonic flow and a direct solution for the equilibrium load can be obtained.

$$\{\ell\} = q[A]\{\alpha_e\}$$

$[A]$ is the matrix of the aerodynamic influence coefficients.

$$\{\ell\} = q[[I] - q[A][D]]^{-1}[A]\{\alpha_r\}$$

However, for transonic flow with nonlinear aerodynamic relations no such direct solution is possible, but instead an iterative procedure is used. As a first approximation to the wing deformation $\Delta\alpha^{(1)}$, ℓ is substituted by the rigid wing load in Eq. (2), and a corresponding approximation to the elastic wing mean surface slope $\alpha_e^{(1)}$ is obtained from Eq. (3). A flow field that matches this deformed wing better is computed by Eq. (1), and the pressure distribution is used to determine a second approximation of the deformation $\Delta\alpha^{(2)}$ by Eq. (2). The process is repeated until the external aerodynamic loading is in equilibrium with the internal elastic forces.

V. Numerical Procedure

a) Mesh Requirements

The small perturbation potential Eq. (1) is given and solved in Cartesian coordinates and the airplane configuration has to be described in a mesh of straight lines in this coordinate system. Some requirements on the generated mesh have to be fulfilled in order to solve the Eq.(1). The leading edge of each wing has at every y-station to be situated midway between two x-stations. This is hard to meet in Cartesian coordinates in the case of closely coupled canard-wing configurations, unless the canard and the wing have either the same angles of sweep of the leading edges, $\Lambda_{c,w}$, or have no x-

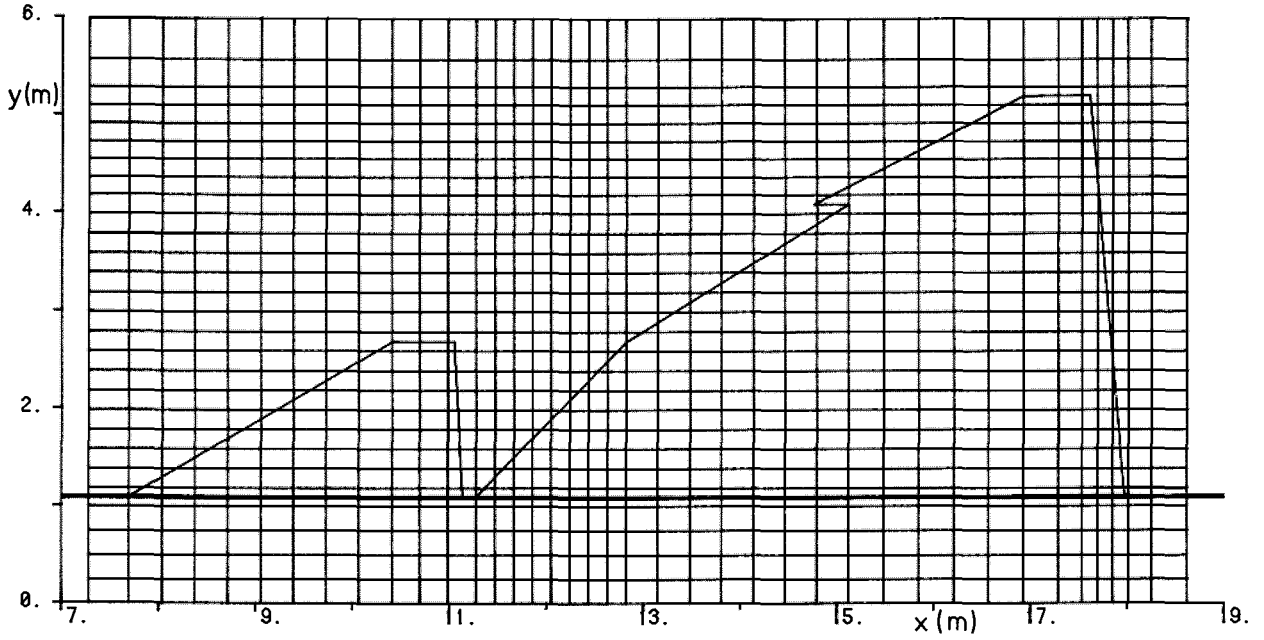

Fig. 1 Fine grid arrangement in the surrounding of the canard-wing configuration.

station in common along with no change in Λ_w behind the whole canard wing. In practice some modifications of the main wing may have to be allowed for in order to produce an acceptable grid for both wings. The projections of the mesh and the studied canard-wing configuration of SAAB 37 Viggen on the z = 0 plane are given in Fig. 1. The tips of canard and main wing are preferably placed midway between two spanwise (y-) stations in order to get proper evaluations of lift and moment. As can be seen from Fig. 1 the distribution of points is rather smooth.

b) Solution Procedure at Subsonic Speed

As mentioned in Section II the successive line over-relaxation procedure is used to solve Eq. (1) in finite difference form. The values of the potential field at the computational points along any vertical line are computed simultaneously. In one relaxation cycle each line is passed once. The outer boundaries are updated after a number of cycles but when better convergence is reached these are updated more often and finally at each cycle.

When the above procedure is applied to an elastic wing and the local angles of attack due to loading have to be evaluated (see Section IV) some relaxation cycles are performed before a new evaluation of the deformation is made. For faster convergence the changes in local angles of attack are usually damped to begin with.

c) Solution Procedure at Supersonic Speed

The solution procedure used at subsonic speed was not satisfactory at supersonic speed. Oscillations appeared and it seemed to be easier to get oscillating than steady solutions. A steady coarse grid solution would tend to develop into an oscillating solution during some 100-200 cycles of the type described in Section b, in the fine grid. A slight oscillation introduced somewhere in the computational grid seemed to spread out in the domain, grow and die out again. This problem was solved by not letting the solution procedure to continue to the next x flow field station until some desired degree of convergence had been reached at the actual x-station. No limits have been specified on how many times an x-station can be iterated but, when the desired degree of convergence is reached the iterative procedure is continued at the next x-station. One relaxation cycle means here passing each x-station at least once. Before starting a relaxation cycle and after finishing it the local angles of attack due to loading are evaluated. The number of cycles necessary for convergence varies but in no case has less than 14 cycles been carried out. The required degree of flow field convergence is increased from one cycle to the next during the first few cycles performed for each case.

VI. Results

The SAAB 37 Viggen was selected because information on its aeroelastic behaviour was available and its complexity offered a challenge to the method.

The airplane is approximated with a wing-body combination consisting of a cylindrical body with a pointed nose, a high mounted canard and a low mounted main wing. All computations - except preparation of the deformation matrix - were

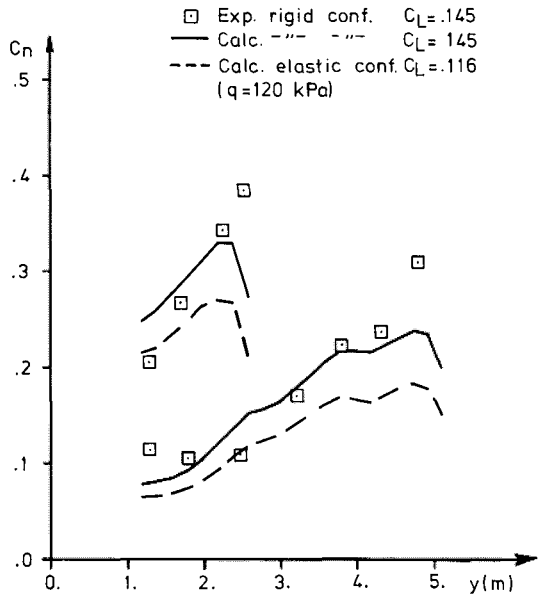

Fig. 2. Spanwise normal force distribution at $M_\infty = 0.9$, $\alpha = 2.865°$ and $\delta = 0°$.

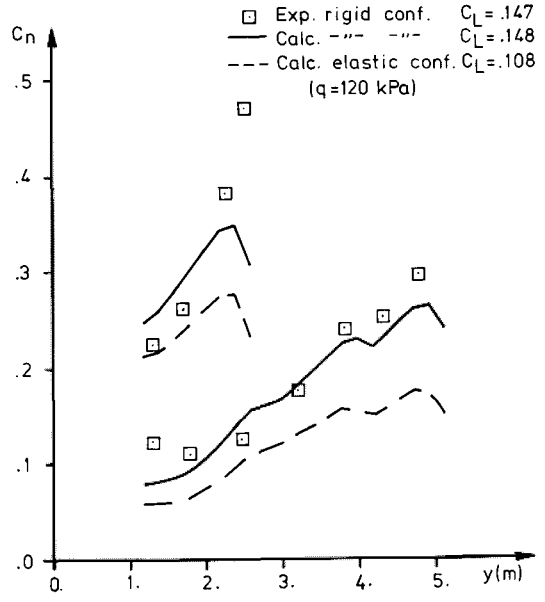

Fig. 3. Spanwise normal force distribution at $M_\infty = 1.1$, $\alpha = 2.865°$ and $\delta = 0°$.

performed on a CDC CYBER 175 computer (in Stockholm). The aeroelastic matrix was delivered by the SAAB company and produced on one of their VAX machines. The finest grid that could be stored in the actual computer was 57×36×40 = 82080 points which meant that the canard was described by 52 quite equally spaced points while the main wing was described by 280 points. The fine mesh for the canard-wing configuration is shown in Fig. 1.

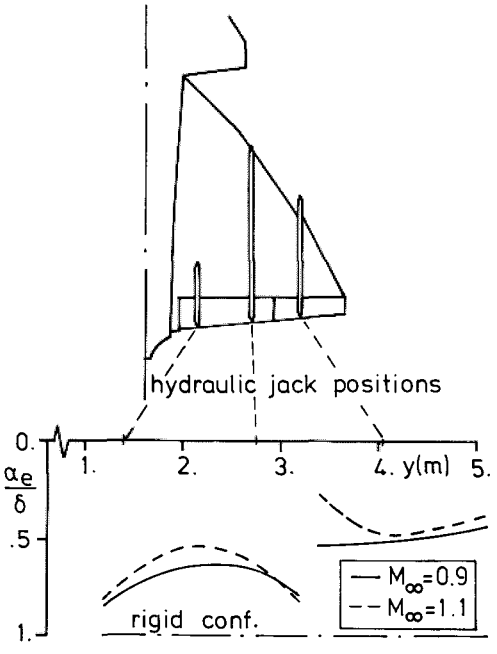

Fig. 4. Comparison of local slopes α_e/δ at the trailing edge of the main wing for M_∞=0.9 and 1.1, α=0°, δ=2.865°, q=60 kPa.

The computations have been performed at M_∞ = 0.9 and 1.1 with three different combinations of small angles of attack and angles of elevon; α = 0°, δ = 0°; α = 0°, δ = 2.865°; α = 2.865°, δ = 0°. All these combinations have been run at different q-values, including q = 0. In addition there were four cases run at M_∞ = 0.7 and two at M_∞ = 1.4. Consequently a considerable amount of data is available.

Figs. 2 and 3 show the spanwise distribution of normal forces at α = 2.865°, δ = 0° at M_∞ = 0.9 and 1.1 resp. The agreement at q = 0 with values evaluated from pressure measurements on a rigid wing in wind tunnel is very good. The computed values close to the body are somewhat higher for the canard and lower for the main wing. The computed total lift for the wings is in excellent agreement with the experimental total lift for the wings - see C_L values written at notation explanations in Figs. 2 and 3.

Fig. 4 shows the local angles of attack, α_e, at the last computational grid point on the main wing at each section for the case α = 0° and δ = 2.865° at M_∞ = 0.9 and 1.1. The elevon command system is shown in the same figure in order to demonstrate how the spanwise variation of α_e/δ reflects the support of the elevon by three hydraulic jacks. The major difference due to Mach number is seen at the inner part of the outer elevon which also can be expected from the larger hinge moment at the higher Mach number.

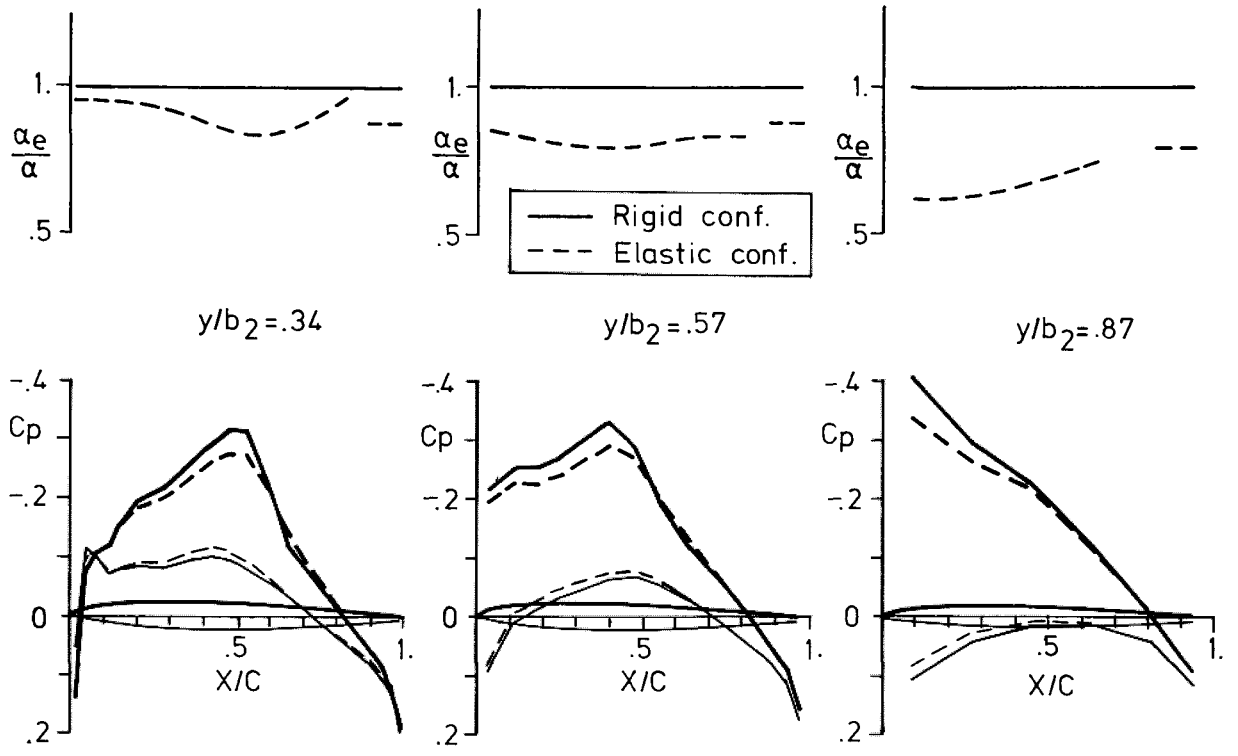

Fig. 5. Wing surface pressures for rigid and elastic (q = 60 kPa) configurations at $M_\infty = 0.9$, $\alpha = 2.865°$ and $\delta = 0°$.

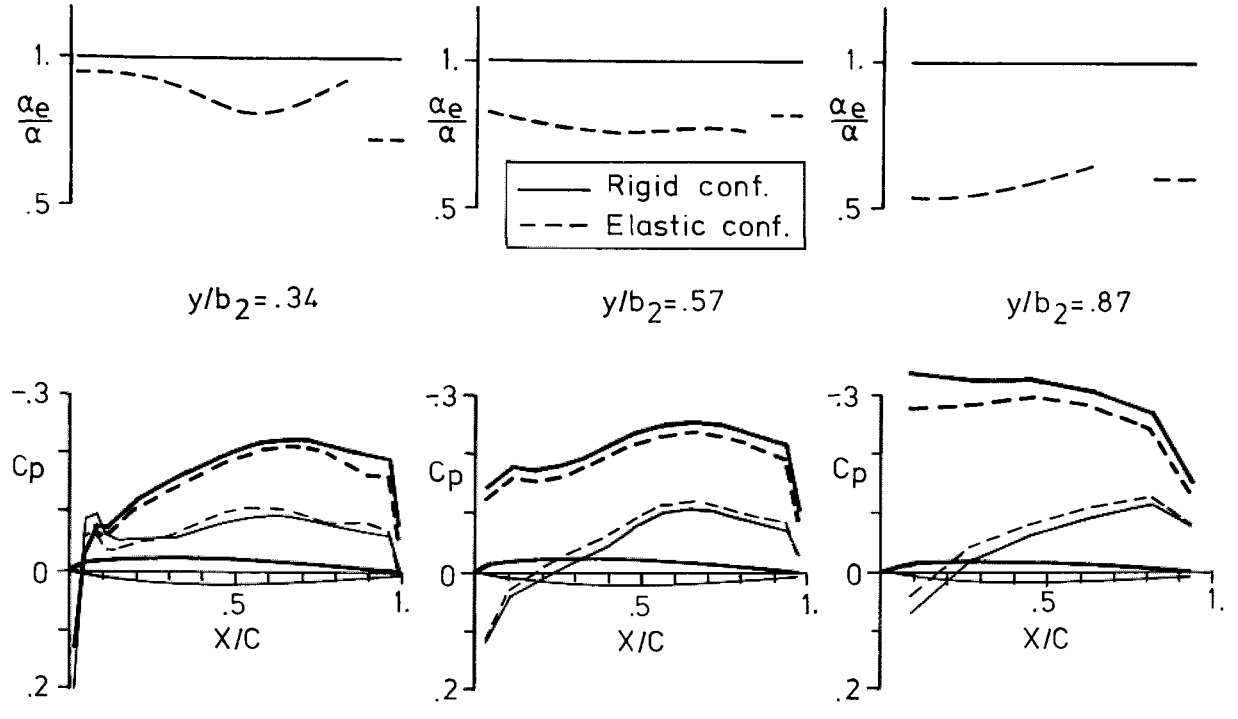

Fig. 6. Wing surface pressures for rigid and elastic (q = 60 kPa) configurations at $M_\infty = 1.1$, $\alpha = 2.865°$ and $\delta = 0°$.

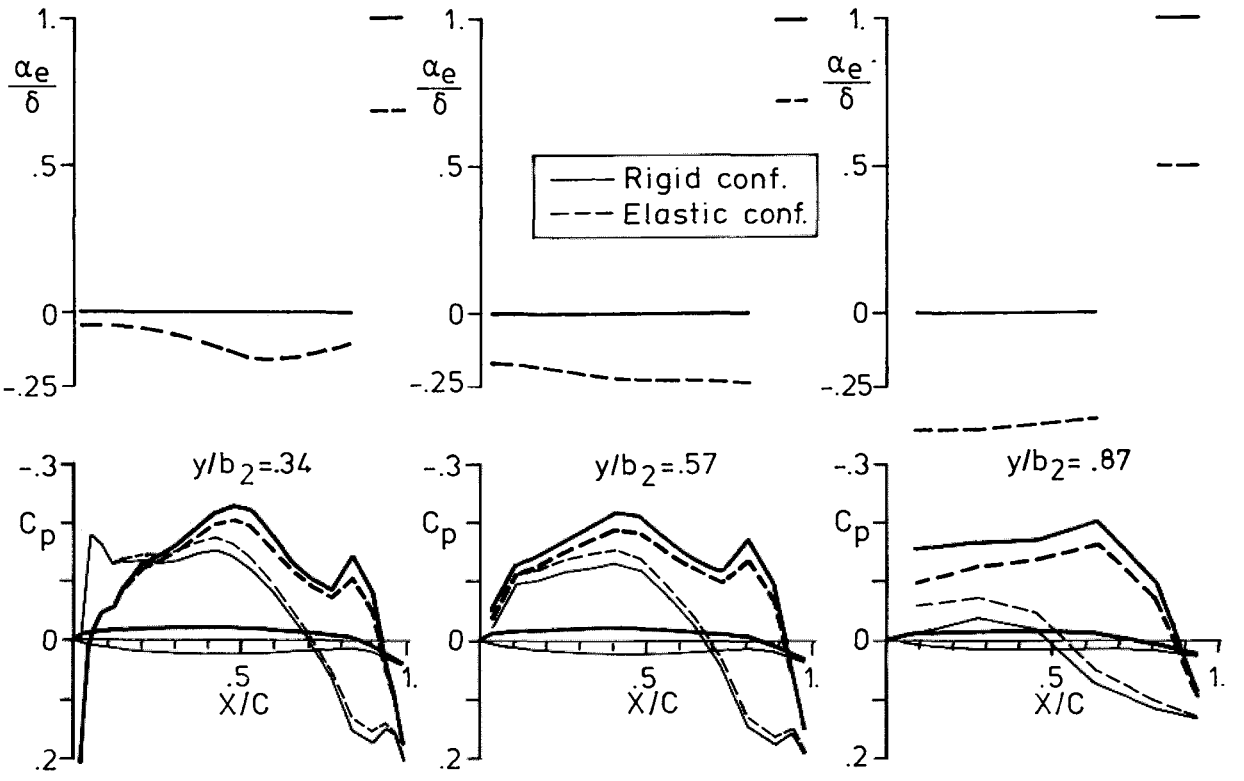

Fig. 7 Wing surface pressure for rigid and elastic (q = 60 kPa) configurations at $M_\infty = 0.9$, $\alpha = 0°$ and $\delta = 2.865°$

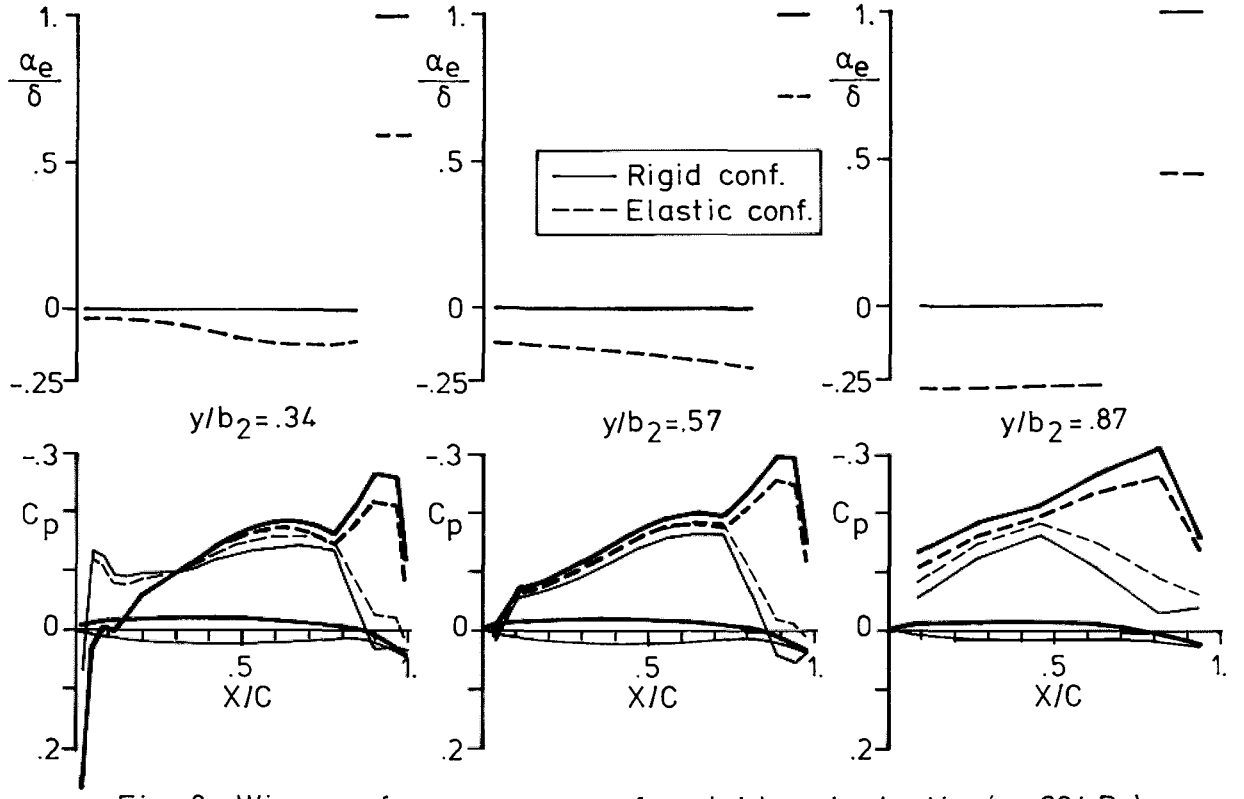

Fig. 8 Wing surface pressures for rigid and elastic (q = 60 kPa) configurations at $M_\infty = 1.1$, $\alpha = 0°$ and $\delta = 2.865°$

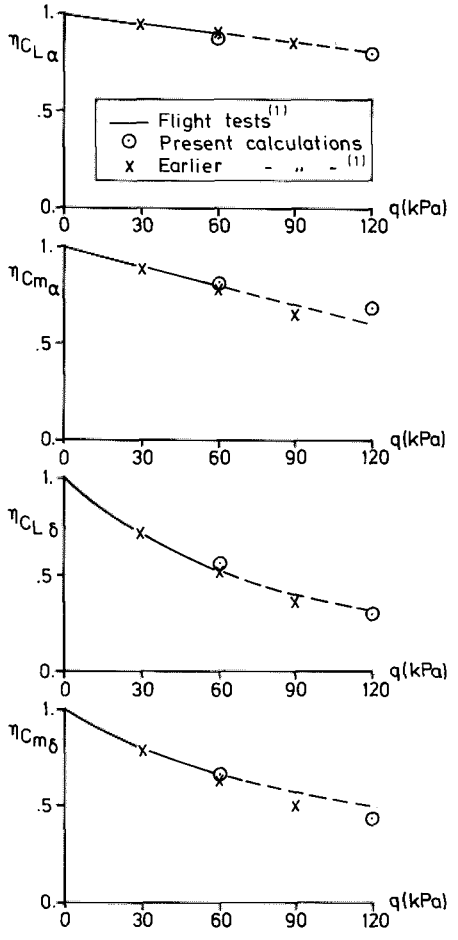

Fig. 9. Aerodynamic effectiveness parameters at M_∞=0.9.

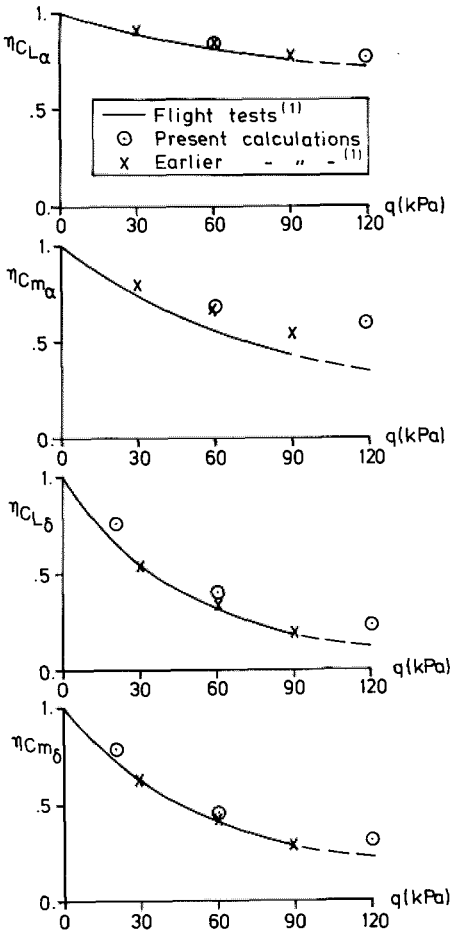

Fig. 10. Aerodynamic effectiveness parameters at M_∞=1.1.

Fig. 5 presents computed pressure distributions at M_∞ = 0.9, α = 2.865° and δ = 0° at three span (y-) stations. The main wing span stations chosen to be shown are situated behind the canard, just outside the canard and outside the saw-tooth of the main wing. Above each pressure plot the change of local angles of attack due to the elastic effects can be seen. The dashed lines in all plots are the values computed at q equals 60 kPa. The elasticity of the wing causes in this case the local angles of attack to be smaller than the actual angle of attack (= 2.865°) by up to 40%. Fig. 6 contains the same information as Fig. 5 but at M_∞ = 1.1.

Fig. 7 presents some results for the case α = 0°, δ = 2.865° at M_∞ = 0.9, while Fig. 8 shows the corresponding results at M_∞ = 1.1. The dashed line describing the local angles of attack should be compared with the broken line situated at level 0 and at level 1. Level 1 shows where the elevon (deflection angle δ = 2.865°) is situated. Very large deflections and load reductions can be seen due to elastic effects. The efficient angle of elevon is reduced and the reduction is as large as 30%.

Integration of the pressure distributions gives coefficients for lift and pitching moment. In order to compare the coefficients for the elastic wing at different dynamic pressures a parameter, here called elastic effectiveness, η, is introduced. The case of the rigid wing is represented by the dynamic pressure being equal to zero.

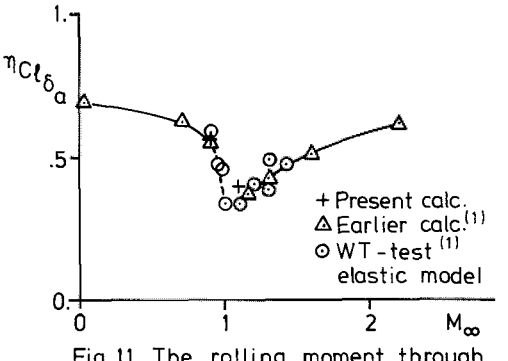

Fig. 11. The rolling moment through the transonic speed range (1)

Four different effectiveness parameters, $\eta_{C_{L_\alpha}}$, $\eta_{C_{m_\alpha}}$, $\eta_{C_{L_\delta}}$ and $\eta_{C_{m_\delta}}$ have been computed for all cases treated. $\eta_{C_{L_\alpha}}$ is defined as

$$\eta_{C_{L_\alpha}} = \frac{(C_{L_\alpha})_{elastic}}{(C_{L_\alpha})_{rigid}}$$

and the other η's are defined in the same manner. Fig. 9 contains the results for the four η's at $M_\infty = 0.9$ and shows a comparison of present results with earlier computations with linearized theory and tests. Fig. 10 presents the corresponding results at $M_\infty = 1.1$. At $M_\infty = 0.9$ the agreement is very good for all four effectiveness parameters shown while the results at $M_\infty = 1.1$ are quite similar to the results obtained from earlier calculations with linearized theory.

Finally the rolling moment, $C_{\ell_{\delta_a}}$, has been evaluated at $M_\infty = 0.9$ and $M_\infty = 1.1$ for $q = 60$ kPa. The values obtained have been indicated in Fig. 11 showing the variation of $C_{\ell_{\delta_a}}$ through the transonic speed range. The rolling moment at $M_\infty = 0.9$ is on the curve of Fig. 11 while at $M_\infty = 1.1$ it is somewhat off that curve.

VII. Conclusions

A transonic small perturbation (TSP) method has been modified for calculations of canard/tail configurations. As an option to the program the possibility of evaluating aeroelastic effects has been implemented. The aeroelastic deformation is obtained by balancing aerodynamic loads against interior forces.

The results presented here show that aeroelastic characteristics can be predicted in the applicability domain of the transonic small perturbation equation even for such a complicated configuration as SAAB 37 Viggen. A special effort has been made to calculate the characteristics at $M_\infty = 1.1$.

VIII. References

(1) Kloos, J., Elmeland, S.G.L.: "Static Aeroelastic Effects on the Aerodynamics of the SAAB 37 Viggen Aircraft, a Comparison between Calculations, Wind Tunnel Tests and Flight Tests". ICAS Paper No. 74-55, The 9th Congress of the ICAS, Haifa, Israel, August 25-30, 1974.

(2) Shankar, V., Malmuth, N.: "Computational Treatment of Transonic Canard-Wing Interactions", AIAA-Paper 82-0161, AIAA 20th Aerospace Sciences Meeting, Orlando, Florida, January 11-14, 1982.

(3) Murman, E.M., Cole, J.D.: "Calculation of Plane Steady Transonic Flows", AIAA Journal, Vol. 9, No. 1, 1971.

(4) Schmidt, W.: "A Self-Consistent Formulation of the Transonic Small-Disturbance Theory". Recent Developments in Theoretical and Experimental Fluid Mechanics edited by U. Müller, K.G. Roesner, B. Schmidt, Springer-Verlag, Berlin, Heidelberg, 1979.

(5) Klunker, E.R.: "Contribution to Methods for Calculating the Flow about Thin Lifting Wings at Transonic Speeds. Analytical Expressions for the Far Field", NASA TN D-6530, 1971.

Acknowledgements

This investigation has been financed by the Air Material Department of the Swedish Defence Material Administration under Contract Nos. AU-1540 and AU-1691.

The authors wish to express their gratitude to Lorentz Elmeland of SAAB-SCANIA AB for valuable discussions and suggestions during the course of this work and to personnel at SAAB-SCANIA and FFA for their assistance.